ON THE DYNAMICS OF DUST-ACOUSTIC AND DUST-CYCLOTRON FREAK WAVES IN A MAGNETIZED DUSTY PLASMA

N. AKHTAR[1,2,a], S. A. EL-TANTAWY[3,4,b], S. MAHMOOD[1,2,c], ABDUL-MAJID WAZWAZ[5,d], HAFEEZ UR-REHMAN[1], AMAN-UR-REHMAN[2]

[1]Theoretical Physics Division (TPD), PINSTECH, P.O. Nilore, Islamabad 45650, Pakistan
[a]Email: naseem_qau@yahoo.com
[2]Department of Physics and Applied Mathematics (DPAM), PIEAS, P.O. Nilore, Islamabad 45650, Pakistan
[c]Email: *shahzadm100@gmail.com*
[3]Research Center for Physics (RCP), Department of Physics, Faculty of Science and Arts, Al-Mikhwah, Al-Baha University, Saudi Arabia
[b]Corresponding author Email: *samireltantawy@yahoo.com*
[4]Department of Physics, Faculty of Science, Port Said University, Port Said 42521, Egypt
[5]Department of Mathematics, Saint Xavier University, Chicago, IL 60655, USA
[d]Email: *wazwaz@sxu.edu*

Compiled July 29, 2018

Abstract. The modulational instability of dust-acoustic wave (DAW) and dust-cyclotron wave (DCW) in a three-component plasma that consists of dust, ions, and electrons in a magnetized dusty plasma is investigated. Moreover, the freak/rogue waves creation and propagation of DAW and DCW in the present plasma system are reported. Electrons and ions both follow the Maxwellian distribution, while the negatively charged dust is taken to be dynamic. For studying MI, a nonlinear Schrödinger equation (NLSE) is obtained using the Krylov-Bogoliubov-Mitropolsky method. The MI criterion for the NLSE is defined precisely and investigated numerically for DAW and DCW. The stable and unsteady regions of the modulated wave packets were accurately quantified based on the relevant physical parameters. The effects of relevant physical parameters namely, the magnetic field intensity, electron to dust density concentration ratio, ratios of effective temperature to electrons and ions temperature, and angle of wave propagation on both stable and unstable regions of DAW and DCW are examined numerically. It is found that, within unstable regions, a random perturbation of the amplitude grows and thus leads to a creation of freak/rogue waves. In order to demonstrate the effects of the physical parameters on the rogue waves (RWs) profile, the relevant numerical analysis of the rational solution of the NLSE is presented. Also, the higher-order solutions/or the super RWs are reported. The possible observation of propagation of fundamental RWs and super RWs in space plasmas and in laboratory experiments is also pointed out.

Key words: Nonlinear Schrödinger Equation, Modulational Instability, Envelope Solitons, Magnetized Dusty Plasma, Freak Waves.

1. INTRODUCTION

The study of dusty plasma has gained interest in the last few decades due to its observations [1–3] and applications [4] in the space and laboratory. The size of the dust charged particles varies from millimeters to micrometers, and their mass lies in the range $10^6 - 10^{12}$ of proton mass and most of the time they are negatively charged of the order of $10^3 - 10^6$ times the electronic charge [5, 6]. The dust particles appear as impurities and drastically affect the behavior of the surrounding plasma in the laboratory [7]. Many authors studied the linear [8, 9] and nonlinear [10, 11] electrostatic wave in the presence [8] and absence [9–11] of the external magnetic field. The presence of the charged dust grains in the plasma would modify the collective behavior of a plasma and some new modes excite on the same time as well [12–14]. For instance, Rao *et al*. [15] predicted theoretically the existence of dust-acoustic wave (DAW) in an unmagnetized plasma that has inertial dust and Maxwellian distributed electrons and ions. In such mode dust charged particles provide the inertia and the restoring force is provided by inertialess electrons and ions. Shukla and Silin [16] showed the existence of dust-ion acoustic wave (DIAW) theoretically and it was confirmed experimentally later on by Barkan *et al.* [3]. The different laboratory experiments on dusty plasmas have confirmed the existence of dust-acoustic wave (DAW) and dust-ion acoustic wave (DIAW) [3, 17, 18]. Akhtar *et al.* [19] studied the dust-acoustic solitary waves in the presence of hot and cold dust while electrons and ions follow the Boltzmann distribution.

Numerous authors investigated the propagation of nonlinear electrostatic and electromagnetic structures in dusty plasmas [4, 20–27]. The propagation of envelope waves (wave packets) in a dispersive nonlinear medium such as plasmas, is known to be subjected to the amplitude modulation due to intrinsic medium nonlinearity. The envelope structures, which contains both fast and slow oscillations, can be obtained when nonlinearity balances with the wave group dispersion effects in the system. The envelope structures such as solitons and breathers are localized modulated wave packets whose dynamics are governed by a nonlinear Schrödinger equation (NLSE). The methods that used to investigate such mechanism are a reductive perturbation technique (RPT) [22–26] or the Krylov-Bogoliubov-Mitropolsky (KBM) method [28–31] leading to derivation of a NLSE. The NLSE is a partial differential equation (PDE) that has been used to study the modulational instability (MI) of the nonlinear structures in nonlinear dispersive media [32, 33].

Many nonlinear structures can be generated in plasma physics. One of these structures is the rogue/freak waves [34]. Rogue waves (RWs) are ‘spontaneous’ and short-lived phenomena appearing suddenly out of normal waves and disappear without a trace. Freak wave (FW) is an unusually wave and its amplitude can reach more than twice the value of the surrounding waves. Moreover, its appearance statistics

deviates from the Gaussian distribution by exhibiting 'heavy tails' in the probability density function [35]. To explain its unexpected emergence, a number of mechanisms have been suggested. It is found that the linear approach is unsuitable to describe the RWs generation. One of the essential mechanisms involve interactions of individual solitons or solitons with the plane wave. The most direct approaches that used to modeling rogue waves is related to the development of MI, which is associated with the growth of perturbations on a plane wave background. Furthermore, the appearance of the super RWs (higher-order RWs) has been attributed to the interactions of elementary solitons on finite background (SFBs). Fundamental and super RWs are investigated in many physical situations such as in oceanography, nonlinear fiber optics, optical systems, optical cavities, parametrically driven capillary waves, the atmosphere, and in plasmas [36–46]. Therefore, understanding the origin of RWs and their propagation in dusty plasmas gives us a glimpse about the presence of highly energetic pulses that propagate in these environments. Shalini *et al.* [47] investigated the amplitude modulation of three dimensional (3D) DIAWs in a magnetized three-component dusty plasma that has dynamic ions, kappa distributed electrons, and stationary dust. Guo and Mei [48] explored the dust-ion acoustic wave (DIAW) and MI in a magnetized plasma which has positive and negative ions, kappa distributed electrons, and immobile charged dust particles. It is found that the magnetic field intensity modified the unstable regimes of modulated DIAW. Akhtar *et al.* [49] investigated the MI of dust-ion acoustic wave (DIAW) and dust-ion cyclotron wave (DICW) via deriving the NLSE using the KBM method in a dusty plasma that has dynamic ions, nonthermal electrons and static positively and negatively charged dust particles. Zhang *et al.* [20] studied numerically the one-dimensional (1D) RWs in a dusty plasma consisting of mobile negative dust particles with Maxwellian electrons and positive ions using particle-in-cell method [20]. According to the best of our knowledge, the investigation of MI of DAWs and associated RWs-types in a magnetized dusty plasma with Maxwellian distributed electrons and ions using the KBM method has not yet been done before. In this paper, we extend the work of Zhang *et al*. [20] to investigate the MI and RWs in a magnetized dusty plasma having Maxwellian distributed electrons and ions.

The structure of the paper is organized as follows: In Sec. 2, the basic set of fluid equations in the presence of magnetic field are presented for negatively charged dynamic dust with Maxwellian distributed electrons and ions. In Sec. 3, the NLSE is derived using the KBM perturbation method. In Sec. 4, the analytical and numerical study of modulational instability of dust-acoustic and dust-cyclotron waves is carried out. Using the rational solution of the NLSE, the nonlinear evolution of the FWs/RWs of DAW and DCW has been investigated numerically in magnetized dusty plasmas. Finally, a summary of the obtained results and their applications is presented in Sec. 5.

2. SET OF DYNAMIC EQUATIONS

The propagation of nonlinear dust-acoustic structures in a collisionless, magnetized dusty plasma whose constituents are distributed electrons and ions, and fluid negatively charged dust grains is considered. It is assumed that the collisions of dust grains with electrons, ions, and neutral particles are negligible due to the extremely massive of the dust grains. On the slow dust motion time scale, the electrons and ions are approximately local thermodynamic equilibrium and therefore follow the Maxwellian velocity distribution function. It is assumed that the magnetic field is along the z-direction, *i.e.*, $B_0 = B_0\hat{z}$, whereas the propagation vector makes an angle θ with the z-axis and lies in the xz-plane. The nonlinear dynamics of electrostatic waves in magnetized dusty plasmas is governed by the following fluid equations:

$$\frac{\partial n_d}{\partial t} + \nabla.\left(n_d \mathbf{u}_d\right) = 0, \tag{1}$$

$$\frac{\partial \mathbf{u}_d}{\partial t} + \left(\mathbf{u}_d.\nabla\right)\mathbf{u}_d = -\frac{Z_d e}{m_d}\left(\mathbf{E} + \frac{1}{c}\mathbf{u}_d \times \mathbf{B}_0\right). \tag{2}$$

The electrons and ions follow the Boltzmann distribution as

$$n_e = n_{e0} e^{e\varphi/T_e}, \tag{3}$$

$$n_i = n_{i0} e^{-e\varphi/T_i}. \tag{4}$$

The system is closed with the help of Poisson's equation

$$\nabla \cdot \mathbf{E} = 4\pi e\left(n_i - n_e - Z_d n_{d0}\right). \tag{5}$$

The charge neutrality condition at equilibrium is given by

$$n_{e0} + Z_d n_{d0} = n_{i0}. \tag{6}$$

Here, m_d is the mass of the charged dust grain moving with velocity:

$$u_d \equiv (u_{dx}, u_{dy}, u_{dz})$$

and n_d is its unnormalized number density. The unnormalized densities of the electrons and ions are n_e and n_i, respectively. The equilibrium number densities of dust particles, Maxwellian ions and electrons are, respectively, n_{d0}, n_{i0}, and n_{e0}. The dust charge number is denoted by Z_d. Here, T_e and T_i stand for the temperatures of the electrons and the positive ions, respectively, under the assumption $T_{e,i} >> T_d$, the thermal effect of dust charged grains is neglected because the dust dynamics has been taken up under cold approximation. The electric field is $E = -\nabla\varphi$, where φ is the unnormalized electrostatic potential. The equilibrium number densities of dust particles, ions, and electrons are n_{d0}, n_{i0}, and n_{e0}, respectively.

We define a new axis ξ in the xz-plane along the direction of propagation of the electrostatic waves in a magnetized plasma [50]. The wave vector is $k = k\hat{\xi}$ and

the operator $\nabla = \hat{\xi}\partial_{\xi}$, where $\hat{\xi} = \hat{x}\sin\theta + \hat{z}\cos\theta$ is the unit vector along the direction of propagation of the wave.

The normalized set of dynamic equations in the component form can be written as

$$\frac{\partial n_d}{\partial t} + \frac{\partial (n_d u_\xi)}{\partial \xi} = 0, \tag{7}$$

$$\frac{\partial u_{dx}}{\partial t} + u_\xi \frac{\partial u_{dx}}{\partial \xi} = \sin\theta \frac{\partial \Phi}{\partial \xi} - \frac{u_{dy}}{\mu}, \tag{8}$$

$$\frac{\partial u_{dy}}{\partial t} + u_\xi \frac{\partial u_{dy}}{\partial \xi} = \frac{u_{dx}}{\mu}, \tag{9}$$

$$\frac{\partial u_{dz}}{\partial t} + u_\xi \frac{\partial u_{dz}}{\partial \xi} = \cos\theta \frac{\partial \Phi}{\partial \xi}, \tag{10}$$

$$n_e = \delta e^{\alpha\Phi}, \tag{11}$$

$$n_i = (1+\delta)\, e^{-\beta\Phi}, \tag{12}$$

where $\delta = n_{e0}/Z_d n_{d0}$, $\alpha = T_{eff}/T_e$ and $\beta = T_{eff}/T_i$ are defined.

The Poisson's equation is described as

$$\frac{\partial^2 \Phi}{\partial \xi^2} = \delta e^{\alpha\Phi} + n_d - (1+\delta)\, e^{-\beta\Phi}. \tag{13}$$

The normalized density of electrons and ions are n_e and n_i. Here normalization of independent and dependent variables is defined as $t^{'} \longrightarrow t\omega_{pd}$, $\nabla^{'} \longrightarrow \lambda_D \nabla$, $n_j^{'} \longrightarrow n_j/Z_d n_{d0}$, $(j = e, i, d)$, $u_d^{'} \longrightarrow u_d/C_{sd}$, $\Phi \longrightarrow e\varphi/T_{eff}$, where

$$T_{eff} = Z_d n_{d0} T_i T_e / \left(n_{e0} T_i + n_{i0} T_e\right)$$

is the effective temperature, $C_{sd} = \sqrt{Z_d T_{eff}/m_d}$ is the dust-acoustic speed, $\omega_{pd} = \sqrt{4\pi Z_d n_{d0} e^2/m_d}$ is the dust plasma frequency, $\lambda_D = \sqrt{T_{eff}/(4\pi Z_d n_{d0} e^2)}$ is the system's Debye length, respectively, so that $C_{sd} = \omega_{pd}\lambda_D$ holds in this model. Here $\mu = \omega_{pd}/\Omega_{cd}$ is the ratio of dust plasma frequency to dust-cyclotron frequency, where $\Omega_{cd} = Z_d e B_0/m_d c$ is the dust-cyclotron frequency. The ' sign that appears in the superscript of the normalized variables has been removed in Eqs.(7-13) and also in further calculations for simplicity. The fluid velocity in the oblique direction in the new axis $\hat{\xi}$ is assumed as

$$u_\xi = u_{dx}\sin\theta + u_{dz}\cos\theta. \tag{14}$$

3. KBM METHOD AND DERIVATION OF A NLSE

In this Section, Krylov-Bogoliubov-Mitropolsky (KBM) method is used to derive a NLSE [51]. The perturbation solution is assumed in the following way:

$$S = S_0(a, \bar{a}, \psi) + \epsilon S_1(a, \bar{a}, \psi) + \epsilon^2 S_2(a, \bar{a}, \psi) + \epsilon^3 S_3(a, \bar{a}, \psi) + ... \tag{15}$$

Here, $S = (n_d, u_{dx}, u_{dy}, u_{dz}, u_\xi, \Phi)^T$ is the state of the system at a given position x and time t and $S^0 = (1,0,0,0,0,0)^T$ is the unperturbed values of the system, a is the complex amplitude and $\bar{a}$ its conjugate. The parameter ϵ ($<< 1$) is a real and small parameter, while superscript T stands for the transpose. The wave phase carrier "ψ" is defined as $\psi = k\xi - \omega t$, where ω and k are, respectively, normalized frequency and wave vector. In Eq. (15) a, $\bar{a}$, and ψ in the bracket show that all the variable quantities n_d, u_{dx}, u_{dy}, u_{dz}, u_ξ, and Φ depend on x and t through a, $\bar{a}$, and ψ, which gives

$$\frac{\partial S}{\partial t} = \frac{\partial a}{\partial t}\frac{\partial S}{\partial a} + \frac{\partial \bar{a}}{\partial t}\frac{\partial S}{\partial \bar{a}} + \frac{\partial \psi}{\partial t}\frac{\partial S}{\partial \psi}, \tag{16}$$

$$\frac{\partial S}{\partial \xi} = \frac{\partial a}{\partial \xi}\frac{\partial S}{\partial a} + \frac{\partial \bar{a}}{\partial \xi}\frac{\partial S}{\partial \bar{a}} + \frac{\partial \psi}{\partial \xi}\frac{\partial S}{\partial \psi}. \tag{17}$$

$$\frac{\partial a}{\partial t} = \sum_{l=1}^{\infty} \epsilon^l A_l(a, \bar{a}), \tag{18}$$

$$\frac{\partial a}{\partial \xi} = \sum_{l=1}^{\infty} \epsilon^l B_l(a, \bar{a}). \tag{19}$$

The unknown functions A_1, A_2, A_3... and B_1, B_2, B_3... that appear in Eqs. (18-19) can be determined using Eqs. (16-17), when we make the solution (15) secularity free.

Substituting the above expressions into the normalized set of Eqs. (16-19) and collecting the terms in the different powers of ϵ, we can obtain n-orders reduced equations. Collecting the first-order terms, *i.e.*, $O(\epsilon)$, we have the following equations:

$$\omega\frac{\partial n_{d1}}{\partial \psi} - k\frac{\partial u_{\xi 1}}{\partial \psi} = 0, \tag{20}$$

$$\omega\frac{\partial u_{dx1}}{\partial \psi} + k\sin\theta\frac{\partial \Phi_1}{\partial \psi} - \frac{u_{dy1}}{\mu} = 0, \tag{21}$$

$$\omega\frac{\partial u_{dy1}}{\partial \psi} + \frac{u_{dx1}}{\mu} = 0, \tag{22}$$

$$\omega\frac{\partial u_{dz1}}{\partial \psi} + k\cos\theta\frac{\partial \Phi_1}{\partial \psi} = 0, \tag{23}$$

$$-k^2\frac{\partial^2 \Phi_1}{\partial \psi^2} + [\delta\alpha + (1+\delta)\beta]\Phi_1 + n_{d1} = 0. \tag{24}$$

The initial solution Φ_1 is assumed in the following way:

$$\Phi_1 = ae^{i\psi} + \bar{a}e^{-i\psi}. \tag{25}$$

From Eqs. (20-24), we obtain the first-order solution $S_1(a,\bar{a},\psi)$ as follows

$$\begin{bmatrix} \Phi_1 \\ n_{d1} \\ u_{dx1} \\ u_{dy1} \\ u_{dz1} \\ u_{\xi 1} \end{bmatrix} = \begin{bmatrix} 1 \\ -\Gamma \\ N_1/\omega k\sin\theta \\ iN_1/\omega^2\mu k\sin\theta \\ -k\cos\theta/\omega \\ -\omega\Gamma/k \end{bmatrix} ae^{i\psi} + c.c., \tag{26}$$

where, $\Gamma = \delta\alpha + (1+\delta)\beta + k^2$ and $N_1 = k^2\cos\theta - \omega^2\Gamma$.

The dispersion relation for the electrostatic waves in a magnetized dusty plasma is given by

$$\omega^2\Gamma - k^2 + \frac{k^2\sin^2\theta}{1-\mu^2\omega^2} = 0. \tag{27}$$

After simplifying the above dispersion relation, we have

$$A\omega^4 + B\omega^2 + C = 0, \tag{28}$$

where $A = \mu^2\Gamma$, $B = -\left(\Gamma + \mu^2k^2\right)$, and $C = \left(1-\sin^2\theta\right)k^2$.

The two symmetrical real roots are obtained from Eq. (28) for the frequency square ω^2

$$\omega_H^2 = \frac{-B+\sqrt{B^2-4AC}}{2A}, \tag{29}$$

$$\omega_L^2 = \frac{-B-\sqrt{B^2-4AC}}{2A}, \tag{30}$$

where ω_H is the high frequency root of the dust-cyclotron waves (DCWs), *i.e.*, $\omega_H >> \Omega_{cd}$ and ω_L is the low frequency root of dust-acoustic waves (DAWs), *i.e.*, $\omega_L << \Omega_{cd}$.

The second-order terms, *i.e.*, $O\left(\epsilon^2\right)$ give the following reduced equations

$$\omega\frac{\partial n_{d2}}{\partial\psi} - k\frac{\partial u_{\xi 2}}{\partial\psi} = L_1, \tag{31}$$

$$\omega\frac{\partial u_{dx2}}{\partial\psi} + k\sin\theta\frac{\partial\Phi_2}{\partial\psi} - \frac{u_{dy2}}{\mu} = L_2, \tag{32}$$

$$\omega\frac{\partial u_{dy2}}{\partial\psi} + \frac{u_{dx2}}{\mu} = L_3, \tag{33}$$

$$\omega\frac{\partial u_{dz2}}{\partial\psi} + k\cos\theta\frac{\partial\Phi_2}{\partial\psi} = L_4, \tag{34}$$

$$-k^2\frac{\partial^2\Phi_2}{\partial\psi^2} + \left[\delta\alpha + \beta(1+\delta)\right]\Phi_2 + n_{d2} = L_5, \tag{35}$$

where

$$L_1 = \left(A_1\partial_a + c.c\right)n_{d1} + \left(B_1\partial_a + c.c\right)u_{\xi 1} + k\partial_\psi\left(n_{d1}u_{\xi 1}\right), \tag{36}$$

$$L_2 = (A_1\partial_a + c.c)\, u_{dx1} - \sin\theta\,(B_1\partial_a + c.c)\,\Phi_1 + k u_{\xi 1}\partial_\psi u_{dx1}, \tag{37}$$

$$L_3 = (A_1\partial_a + c.c)\, u_{dy1} + k u_{\xi 1}\partial_\psi u_{dy1}, \tag{38}$$

$$L_4 = (A_1\partial_a + c.c)\, u_{dz1} - \cos\theta\,(B_1\partial_a + c.c)\,\Phi_1 + k u_{\xi 1}\partial_\psi u_{dz1}, \tag{39}$$

$$L_5 = 2k\,(B_1\partial_a + c.c)\,\partial_\psi\Phi_1 + \left[(1+\delta)\,\beta^2 - \delta\alpha^2\right]\frac{\Phi_1^2}{2}. \tag{40}$$

After tedious mathematical manipulation of Eqs. (31-35), we have

$$\begin{aligned}&\omega^2\left(\omega^2\mu^2D^2+1\right)\left[k^2D^2 - \{\delta\alpha + \beta\,(1+\delta)\}\right]D\Phi_2\\ &+\left(\mu^2\omega^2k^2D^2 + k^2\cos^2\theta\right)D\Phi_2 = X_4,\end{aligned} \tag{41}$$

where $D = d/d\psi$ has been defined and expression for X_4 is given below

$$\begin{aligned}X_4 = {}&\omega\left(\omega^2\mu^2D^2+1\right)L_1 + \omega^2\mu^2k\sin\theta D^2L_2 + \omega\mu k\sin\theta DL_3\\ &+ k\cos\theta\left(\omega^2\mu^2D^2+1\right)L_4 - \omega^2\left(\omega^2\mu^2D^2+1\right)DL_5.\end{aligned} \tag{42}$$

Integrating Eq. (41) with respect to ψ once, we obtain the following nonhomogeneous differential equation

$$\left(y_1D^2 - y_2\right)\left(D^2+1\right)\Phi_2 = \int X_4 d\psi + c_1^{'} = X_5, \tag{43}$$

where

$$\begin{aligned}X_5 = \int X_4 d\psi + c_1^{'} = {}&\omega^3\mu^2DL_1 + \omega\int L_1 d\psi + \omega^2\mu^2k\sin\theta DL_2 + \omega\mu k\sin\theta L_3\\ &+ k\cos\theta\omega^2\mu^2DL_4 + k\cos\theta\int L_4 d\psi - \omega^2\left(\omega^2\mu^2D^2+1\right)L_5 + c_1^{'},\end{aligned} \tag{44}$$

and $y_1 = \mu^2\omega^4k^2$ and $y_2 = \omega^2\left[\delta\alpha + (1+\delta)\,\beta\right] - k^2\cos^2\theta$.

To find the solution for Φ_2, Eq. (26) is used to calculate the expressions of $L_{1\text{-}5}$

$$L_1 = -\left(A_1 + \frac{\omega}{k}B_1\right)\Gamma e^{i\psi} + 2i\omega\Gamma^2a^2e^{2i\psi} + c.c, \tag{45}$$

$$L_2 = (N_2A_1 - \sin\theta B_1)\,e^{i\psi} - i\Gamma\omega N_2a^2e^{2i\psi} + c.c, \tag{46}$$

$$L_3 = \frac{iN_2A_1}{\mu\omega}e^{i\psi} + \frac{N_2\Gamma}{\mu}a^2e^{2i\psi} + c.c + \frac{2N_2\Gamma}{\mu}a\bar{a}, \tag{47}$$

$$L_4 = -\left(\frac{k}{\omega}A_1 + B_1\right)\cos\theta e^{i\psi} + ik\Gamma\cos\theta a^2e^{2i\psi} + c.c, \tag{48}$$

$$L_5 = 2ikB_1e^{i\psi} + \left[\frac{(1+\delta)\,\beta^2 - \delta\alpha^2}{2}\right]a^2e^{2i\psi} + \left[\frac{(1+\delta)\,\beta^2 - \delta\alpha^2}{2}\right]2a\bar{a} + c.c, \tag{49}$$

with $N_2 = \left(k^2\cos\theta - \omega^2\Gamma\right)/\left(\omega k\sin\theta\right)$.

Using expressions (44)-(49) in Eq. (43), we get

$$\begin{aligned}\left(y_1D^2-y_2\right)\left(D^2+1\right)\Phi_2 = i\Big[&\omega\left(A_1+\frac{\omega}{k}B_1\right)\Gamma\left(1-\omega^2\mu^2\right)+\left(1+\omega^2\mu^2\right)k\sin\theta N_2A_1\\ &-\omega^2\mu^2k\sin^2\theta B_1+k\cos^2\theta\left(1-\omega^2\mu^2\right)\left(\frac{k}{\omega}A_1+B_1\right)\\ &-2\omega^2k\left(1-\omega^2\mu^2\right)B_1\Big]e^{i\psi}\\ &+\Big[\omega^2\Gamma^2\left(1-4\omega^2\mu^2\right)+\omega k\sin\theta\Gamma N_2\left(1+2\omega^2\mu^2\right)\\ &+\frac{k^2\cos^2\theta}{2}\left(1-4\omega^2\mu^2\right)\Gamma-\omega^2\left\{\frac{(1+\delta)\beta^2-\delta\alpha^2}{2}\right\}\left(1-4\omega^2\mu^2\right)\Big]a^2e^{2i\psi}\\ &+\left[2\omega k\sin\theta\Gamma N_2-\omega^2\left\{(1+\delta)\beta^2-\delta\alpha^2\right\}\right]a\bar{a}+c.c+c_1^{'}.\end{aligned} \tag{50}$$

We put the coefficient of $e^{\pm i\psi}$ terms equal to zero in Eq. (50), to get the nonsecularity of the second order solution Φ_2. The nonsecularity condition at the second-order claims that the coefficient of $e^{\pm i\psi}$ terms should be zero, which leads to:

$$A_1+v_gB_1=0. \tag{51}$$

Here, v_g is the group velocity of the DAWs and it is given by

$$v_g=\frac{d\omega}{dk}=\frac{\omega^3}{k}\left[\frac{\left(\omega^2\mu^2-1\right)\left\{\delta\alpha+(1+\delta)\beta\right\}}{\mu^2\omega^4\Gamma-k^2\cos^2\theta}\right]. \tag{52}$$

To obtain the nonsecular solution of Φ_2, the relation (51) is inserted into Eq. (50) and finally we have

$$\left(y_1D^2-y_2\right)\left(D^2+1\right)\Phi_2=X_6, \tag{53}$$

while

$$\begin{aligned}X_6=&\left[\left(1-4\omega^2\mu^2\right)\left[\omega^2\Gamma^2+\frac{k^2\cos^2\theta}{2}\Gamma-\omega^2\left\{\frac{(1+\delta)\beta^2-\delta\alpha^2}{2}\right\}\right]\right.\\ &\left.+\omega k\sin\theta\Gamma N_2\left(1+2\omega^2\mu^2\right)\right]a^2e^{2i\psi}+c_1^{''}+c.c,\end{aligned} \tag{54}$$

and $c_1^{''}=c_1^{'}+\left[2\omega k\sin\theta\Gamma N_2-\omega^2\left\{(1+\delta)\beta^2-\delta\alpha^2\right\}\right]a\bar{a}$.

The complete solution for Φ_2 is obtained by solving Eq. (53) as follows:

$$\Phi_2=Ga^2e^{2i\psi}+b\left(a,\bar{a}\right)e^{i\psi}+c.c+c_1\left(a,\bar{a}\right). \tag{55}$$

For detailed calculations of Φ_2, see the Appendix. Here $b\left(a,\bar{a}\right)$ is an arbitrary function of a and $\bar{a}$ and it is independent of ψ and $c_1\left(a,\bar{a}\right)$ is the arbitrary function that appeared after integration and depends on a and $\bar{a}$. Here, G is defined as

$$G=\frac{3\left(1-5\omega^2\mu^2\right)\Gamma^2+3k^2\mu^2\Gamma+\left(4\omega^2\mu^2-1\right)\left\{(1+\delta)\beta^2-\delta\alpha^2\right\}}{6\left[\left(\Gamma+4k^2\right)\omega^2\mu^2-\left(1+\mu^2\right)k^2\right]}. \tag{56}$$

The complete set of the secularity-free solution of $S_2(a,\bar{a},\psi)$ is expressed as

$$\begin{bmatrix} \Phi_2 \\ n_{d2} \\ u_{dx2} \\ u_{dy2} \\ u_{dz2} \\ u_{\xi 2} \end{bmatrix} = \begin{bmatrix} G \\ G_1 \\ G_2 \\ G_3 \\ G_4 \\ G_5 \end{bmatrix} a^2 e^{2i\psi} + \begin{bmatrix} b(a,\bar{a}) \\ \Xi_1 \\ \Xi_2 \\ \Xi_3 \\ \Xi_4 \\ \Xi_5 \end{bmatrix} e^{i\psi} + c.c + \begin{bmatrix} 0 \\ (1+\delta)\beta^2 - \delta\alpha^2 \\ 2\Gamma N_1/\omega k \sin\theta \\ 0 \\ 0 \\ 2\Gamma N_1/\omega k \end{bmatrix} a\bar{a}$$
$$+ \begin{bmatrix} c_1(a,\bar{a}) \\ -\{\delta\alpha + (1+\delta)\beta\} c_1(a,\bar{a}) \\ 0 \\ 0 \\ c_2(a,\bar{a}) \\ \cos\theta c_2(a,\bar{a}) \end{bmatrix}, \tag{57}$$

where G_{1-5} and Ξ_{1-5} have been defined in the Appendix. Also, $c_2(a,\bar{a})$ is an arbitrary function of a and $\bar{a}$.

Now collecting the third-order $\left(O\left(\epsilon^3\right)\right)$ terms, we obtain the following set of equations

$$\omega\frac{\partial n_{d3}}{\partial\psi} - k\frac{\partial u_{\xi 3}}{\partial\psi} = W_1, \tag{58}$$

$$\omega\frac{\partial u_{dx3}}{\partial\psi} + k\sin\theta\frac{\partial\Phi_3}{\partial\psi} - \frac{u_{dy3}}{\mu} = W_2, \tag{59}$$

$$\omega\frac{\partial u_{dy3}}{\partial\psi} + \frac{u_{dx3}}{\mu} = W_3, \tag{60}$$

$$\omega\frac{\partial u_{dz3}}{\partial\psi} + k\cos\theta\frac{\partial\Phi_3}{\partial\psi} = W_4, \tag{61}$$

$$-k^2\frac{\partial^2\Phi_3}{\partial\psi^2} + [\delta\alpha + (1+\delta)\beta]\Phi_3 + n_{d3} = W_5, \tag{62}$$

where

$$W_1 = (A_1\partial_a + c.c)\, n_{d2} + (A_2\partial_a + c.c)\, n_{d1} + (B_1\partial_a + c.c)\,(n_{d1}u_{\xi 1}) + (B_1\partial_a + c.c)\, u_{\xi 2} + (B_2\partial_a + c.c.)\, u_{\xi 1} + k\partial_\psi\,(n_{d1}u_{\xi 2} + n_{d2}u_{\xi 1}), \tag{63}$$

$$W_2 = (A_1\partial_a + c.c)\, u_{dx2} + (A_2\partial_a + c.c)\, u_{dx1} + u_{\xi 1}(B_1\partial_a + c.c)\, u_{dx1} - \sin\theta\,(B_1\partial_a + c.c)\,\Phi_2 - \sin\theta\,(B_2\partial_a + c.c)\,\Phi_1 + ku_{\xi 1}\partial_\psi u_{dx2} + ku_{\xi 2}\partial_\psi u_{dx1}, \tag{64}$$

$$W_3 = (A_1\partial_a + c.c)\, u_{dy2} + (A_2\partial_a + c.c.)\, u_{dy1} + u_{\xi 1}(B_1\partial_a + c.c.)\, u_{dy1} + ku_{\xi 1}\partial_\psi u_{dy2} + ku_{\xi 2}\partial_\psi u_{dy1}, \tag{65}$$

$$W_4 = (A_1\partial_a + c.c)\,u_{dz2} + (A_2\partial_a + c.c.)\,u_{dz1} + u_{\xi 1}\,(B_1\partial_a + c.c.)\,u_{dz1} - \cos\theta\,(B_1\partial_a + c.c.)\,\Phi_2 - \cos\theta\,(B_2\partial_a + c.c)\,\Phi_1 + k u_{\xi 1}\partial_\psi u_{dz2} + k u_{\xi 2}\partial_\psi u_{dz1}, \tag{66}$$

$$W_5 = \left\{B_1\partial_a\,(B_1\partial_a) + B_1\partial_a\left(\bar{B}_1\partial\bar{a}\right) + c.c\right\}\Phi_1 + 2k\,(B_1\partial_a + c.c)\,\partial_\psi\Phi_2 + 2k\,(B_2\partial_a + c.c)\,\partial_\psi\Phi_1 + \left\{(1+\delta)\,\beta^2 - \delta\alpha^2\right\}\Phi_1\Phi_2 - \left[\frac{(1+\delta)\,\beta^3 + \delta\alpha^3}{6}\right]\Phi_1^3. \tag{67}$$

Using Eq. (26) and Eq. (57) in $O\left(\epsilon^3\right)$ set of Eqs. (58-62), the arbitrary functions $c_1\,(a,\bar{a})$ and $c_2\,(a,\bar{a})$ are calculated by collecting constant terms, which gives the following relations,

$$c_1\,(a,\bar{a}) = \eta_1 a\bar{a} + R_1, \tag{68}$$

$$c_2\,(a,\bar{a}) = \eta_2 a\bar{a} + R_2, \tag{69}$$

where $R_{1,2}$ is constant and $\eta_{1,2}$ is defined in the following way

$$\eta_1 = \frac{\left[3\left\{\delta\alpha + (1+\delta)\,\beta\right\} + k^2\right]\cos^2\theta - v_g^2\left[(1+\delta)\,\beta^2 - \delta\alpha^2\right]}{\cos^2\theta - v_g^2\left[\delta\alpha + (1+\delta)\,\beta\right]}, \tag{70}$$

$$\eta_2 = \cos\theta\left[-\frac{2k\Gamma}{\omega} + \frac{v_g\left[3\left\{\delta\alpha + (1+\delta)\,\beta\right\}^2 + \left\{\delta\alpha + (1+\delta)\,\beta\right\}k^2 - \left\{(1+\delta)\,\beta^2 - \delta\alpha^2\right\}\right]}{v_g^2\left\{\delta\alpha + (1+\delta)\,\beta\right\} - \cos^2\theta}\right]. \tag{71}$$

Collecting the third-order terms from the set of Eqs. (7-13), we obtain the $S_3\,(a,\bar{a},\psi)$ solution. To have $S_3\,(a,\bar{a},\psi)$ solution secular free, we put the coefficient of $e^{\pm i\psi}$ equal to zero:

$$i\,(A_2 + v_g B_2) + \frac{P}{2}\left(B_1\frac{\partial}{\partial a} + \bar{B}_1\frac{\partial}{\partial\bar{a}}\right)B_1 + Q\,|a|^2\,a = Ra. \tag{72}$$

The coefficients P, Q, and R that appear in Eq. (72) are expressed as

$$P = \frac{dv_g}{dk} \equiv 3v_g\left(\frac{v_g}{\omega} - \frac{1}{k}\right) + \frac{4\omega\mu^2 v_g^2}{(\omega^2\mu^2 - 1)}\left[1 - \frac{v_g k\left\{\delta\alpha + (1+\delta)\,\beta + k^2\right\}}{\omega\left\{\delta\alpha + (1+\delta)\,\beta\right\}}\right], \tag{73}$$

$$Q = +\frac{v_g k}{2\left\{\delta\alpha + (1+\delta)\,\beta\right\}}\,(GQ_1 + Q_2) - \frac{\Gamma\omega\left(2\omega^2\mu^2 + 1\right)}{4N_3}Q_3 + Q_4, \tag{74}$$

where Q_{1-4} is defined as,

$$Q_1 = \Gamma\left(3k^2 + \Gamma\right) + \frac{2\Gamma k^2\cos^2\theta}{\omega^2} - \left\{(1+\delta)\,\beta^2 - \delta\alpha^2\right\},$$

$$Q_2 = \frac{3\Gamma\left\{\delta\alpha^2-(1+\delta)\beta^2\right\}}{2}+\left[\Gamma\left\{\delta\alpha+(1+\delta)\beta\right\}-\left\{(1+\delta)\beta^2-\delta\alpha^2\right\}\right]\eta_1 + \frac{(1+\delta)\beta^3+\delta\alpha^3}{2}-\frac{\Gamma^2k^2\cos^2\theta}{\omega^2},$$

$$Q_3 = 2G\left(N_1-3\omega^2k^2\right)+\omega^2\left\{(1+\delta)\beta^2-\delta\alpha^2\right\}-3\Gamma^2\omega^2-\Gamma N_1,$$

$$Q_4 = \Gamma N_1\left(\frac{\Gamma\omega}{2N_3}-\frac{2}{\omega}\right)-k\cos\theta\eta_2,$$

$$R = -k\cos\theta\eta_2-\frac{v_gk}{2\left\{\delta\alpha+(1+\delta)\beta\right\}}\left[\left\{(1+\delta)\beta^2-\delta\alpha^2\right\}-\Gamma\left\{\delta\alpha+(1+\delta)\beta\right\}\right]R_1,$$

and $N_3 = \mu^2\omega^4\Gamma - k^2\cos^2\theta$.

Let us assume $t_2 = \varepsilon^2 t$, $\xi_1 = \varepsilon\xi$, and $\xi_2 = \varepsilon^2\xi$ and using Eqs. (18) and (19), we obtain the following equations

$$A_2 = \frac{\partial a}{\partial t_2}-\frac{A_1}{\varepsilon},\ B_2 = \frac{\partial a}{\partial \xi_2}-\frac{B_1}{\varepsilon}, \tag{75}$$

and

$$\left(B_1\frac{\partial}{\partial a}+\bar{B}_1\frac{\partial}{\partial \bar{a}}\right)B_1 = \frac{\partial^2 a}{\partial \xi_1^2}. \tag{76}$$

Using above relations in Eq. (72), we have

$$i\left(\frac{\partial a}{\partial t_2}+v_g\frac{\partial a}{\partial \xi_2}\right)+P\frac{\partial^2 a}{\partial \xi_1^2}+Q\left|a\right|^2a = Ra. \tag{77}$$

Inserting the following coordinate transformation into Eq. (77):

$$\eta = \frac{1}{\varepsilon}\left(\xi_2-v_gt_2\right) = \xi_1-v_gt_1 = \varepsilon\left(\xi-v_gt\right),$$
$$\tau = t_2 = \varepsilon t_1 = \varepsilon^2 t, \tag{78}$$

we finally get the following one-dimensional NLSE

$$i\frac{\partial a}{\partial \tau}+\frac{P}{2}\frac{\partial^2 a}{\partial \eta^2}+Q\left|a\right|^2a = 0. \tag{79}$$

It is noticed that the linear interaction term Ra has been dropped here for simplicity, as it is not of much important and simply causes a phase shift [51].

4. STABILITY ANALYSIS

To investigate the MI of DAWs and DCWs in a magnetized dusty plasma, the linear stability analysis is used [52, 53]. Depending on this analysis and after some manipulations, the following nonlinear dispersion relation is obtained

$$\Omega^2 = \frac{1}{2}PK^2\left(\frac{1}{2}PK^2-2Q|a_0|^2\right), \tag{80}$$

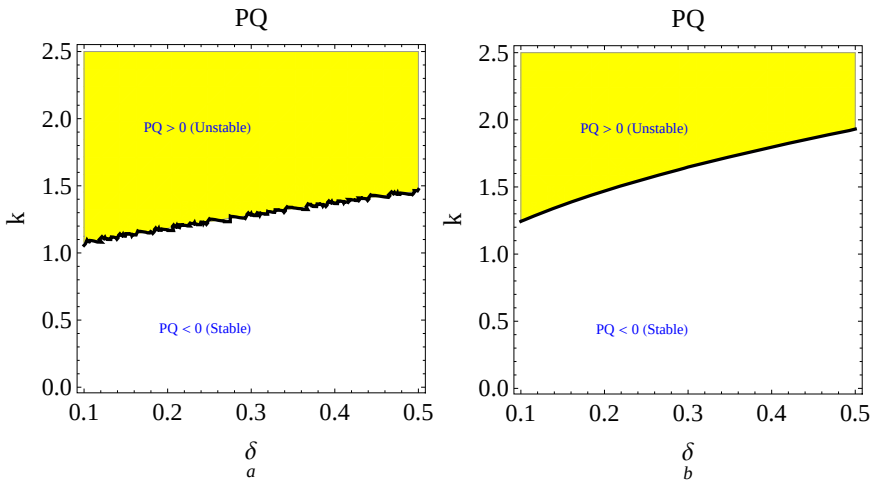

Fig. 1 – (color online) The regions of stable and unstable envelope wave packets according to the sign of the product PQ are depicted against the wave number k and the electron to dust density concentration δ for (a) the slow mode (dust-acoustic mode) and (b) the fast mode (dust-cyclotron mode). Here, $\alpha = 0.5$, $\beta = 0.3$, $\mu = 0.8$, and $\theta = 30^{\circ}$.

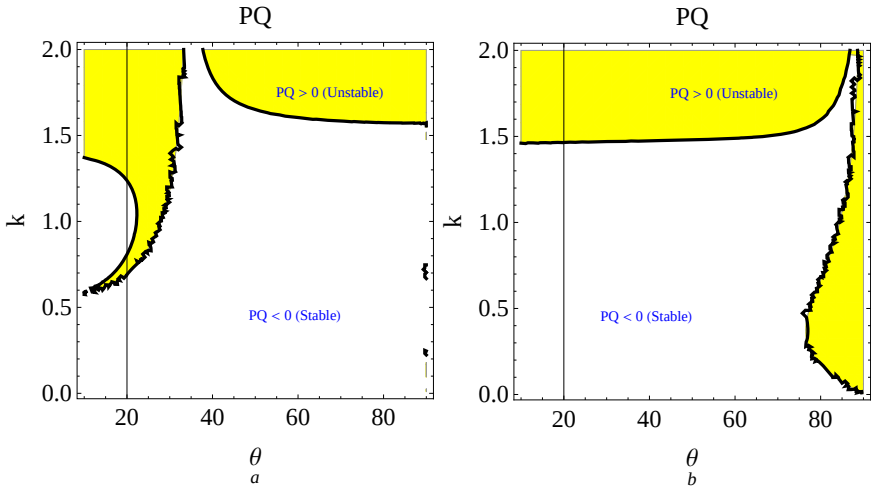

Fig. 2 – (color online) The regions of stable and unstable envelope wave packets according to the sign of the product PQ are depicted against the wave number k and the wave propagation angle θ for (a) the slow mode and (b) the fast mode. Here, $\alpha = 0.5$, $\beta = 0.3$, $\mu = 0.8$, and $\delta = 0.2$.

where $\Omega\,(\ll \omega)$ is the frequency of modulated wave, $K\,(\ll k)$ is the modulational wave number, and a_0 is the normalized carrier wave amplitude.

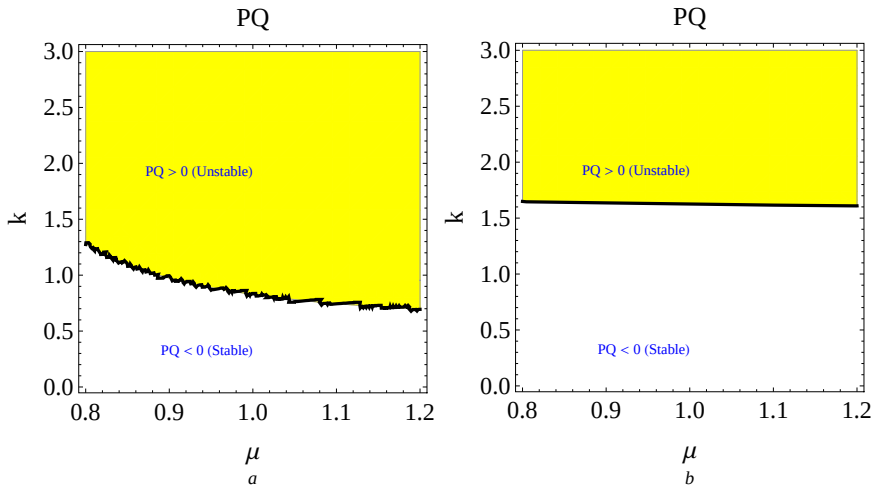

Fig. 3 – (color online) The regions of stable and unstable envelope wave packets according to the sign of the product PQ are depicted against the wave number k and the magnetic field intensity μ for (a) the slow mode and (b) the fast mode. Here, $\alpha = 0.5$, $\beta = 0.3$, $\theta = 30^{\circ}$, and $\delta = 0.3$.

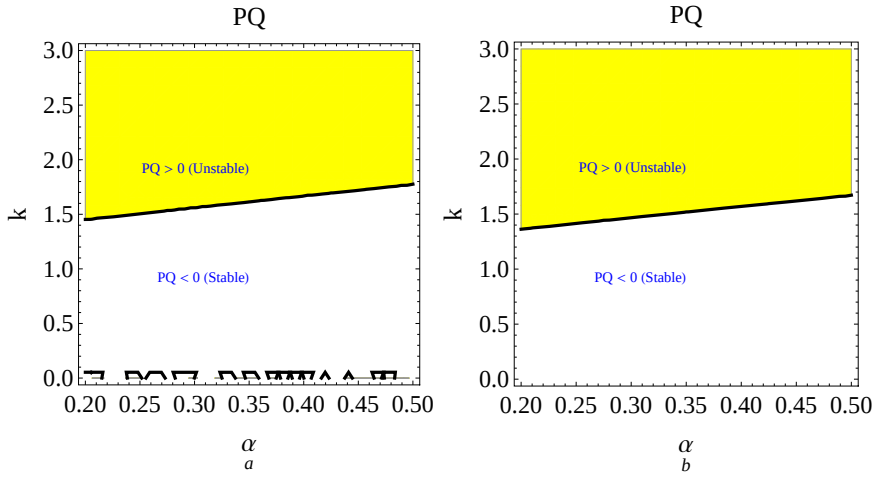

Fig. 4 – (color online) The regions of stable and unstable envelope wave packets according to the sign of the product PQ are depicted against the wave number k and the ratio of the effective temperature to electron temperature α for (a) the slow mode and (b) the fast mode. Here, $\mu = 0.6$, $\beta = 0.3$, $\theta = 30^{\circ}$, and $\delta = 0.3$.

The later relation (80) can be written in the following form

$$\Omega^2 = \left(\frac{1}{2}K^2P\right)^2\left[1 - \frac{K_c^2}{K^2}\right], \tag{81}$$

where $K_c^2 = (4Q/P)\,|a_0|^2$ is the critical value of the modulation wave number. It is shown that the waves become modulationally stable if $PQ < 0$ and in this case Ω is always real for modulational wave number $K\,(\ll k)$ in the region: $K^2 > K_c^2$. On the contrary, for $PQ > 0$, the MI would set in for $K^2 < K_c^2$ and Ω becomes imaginary. In this case, the MI growth rate is given by

$$\Gamma = \mathrm{Im}\,(\Omega) = \frac{1}{2}|P|K^2\sqrt{\left(\frac{K_c^2}{K^2} - 1\right)}. \tag{82}$$

Here, we numerically analyze the possibility of MI of DAWs and DCWs in the presence of magnetic field for the three-component dusty plasma. Equation (80) gives the condition for the MI of obliquely propagating electrostatic waves in a magnetized plasma, which depends on the sign PQ. As the coefficient of dispersion term P is always negative (the figures are not listed here due to the lack of space), a finite amplitude sinusoidal wave is modulationally unstable for $Q < 0$. The solution of NLSE (79) is well documented in the literature and depends on the sign of PQ. For $PQ > 0$, the carrier wave becomes modulationally stable and may propagate in the form of a dark envelope wave packet. On the contrary, for $PQ < 0$, the carrier wave becomes modulationally unstable, which leads to the formation of bright envelope modulated wave packets.

Now, we devote our efforts to examine the effects of various physical parameters on the critical wave number K_c for which $PQ = 0$, which indicates where the MI sets in, or on the sign of the product PQ. The results for both the first (slow) mode ω_L (DAWs, i.e., $\omega_L << \Omega_{cd}$) and the second (fast) mode ω_H (DCWs, i.e., $\omega_H >> \Omega_{cd}$), are investigated in Figs. 1-5. In general, it is noted that the domain of the unstable pulses ($PQ > 0$) is more dominant compared to the domain of stable pulses ($PQ < 0$). Note that the values of the normalized wave number are taken in from 0 to 4, but sometimes we do zoom to demonstrate the effect of the relevant physical parameters. Note that the solid-black line between the white and yellow regions represents the critical wave number K_c, which indicates where the MI sets in. One can notice that the stable pulses can exist only for low wave number values for the two modes. Increasing δ leads to an increase of the wave number K_c or the stable regime and a decrease of the instability domain, which is shown in Fig. 1, i.e., the instability region shifts to higher wave number with the increase of the electron to dust density concentration ratio δ. Also, it is evident from Fig. 1 that the stable region in the fast mode is larger than in the slow one. In Fig. 2a, one observes that for low k values, the DAW becomes stable for all values of the propagation direction θ, but for higher k values, the DAW becomes stable and unstable, *i.e.*, the behavior becomes complex. Figure 2 shows that for $k < 1.5$ and higher values of θ, the region becomes stable for the slow mode but for the fast mode, the region becomes unstable.

Anyway, it is interesting to note that the influence of the propagation direction θ on the critical wave number or the MI is complex. The effect of μ on the MI of the DAW and DCW packets is investigated in Figs. 3a and 3b, respectively. It is obvious that the stable region (or the critical wave number K_c) is shrinking significantly with the increase of μ (*i.e.*, the magnetic field decreases), which means that the dust density effect is more dominant than the magnetic field effect. Also, it is noticed that the stable region for the fast mode is larger than that for the slow one and the critical wave number for slow mode decreases rapidly compared to the fast one. The variation of critical wave number/or the unstable region with effective temperature to electron temperature ratio α is shown in Fig. 4 for $\mu < 1$ (*i.e.*, $\omega_{pd} < \omega_{cd}$). It can be seen from the picture that the unstable region of DAW or DCW shrinks as the value of α is increased. Similarly, the variation of critical wave number/or the unstable region with β is shown in Fig. 5. It is found that the increase of β makes the unstable region narrower, while the stable region becomes wider. Moreover, the increase of β would increase the critical wave number at which the instability sets in and furthermore, expands the stability region. It is noticed here that the instability region for the slow mode is larger than the instability region for the fast mode and MI occurs at low values of k in DAW than in the DCW case.

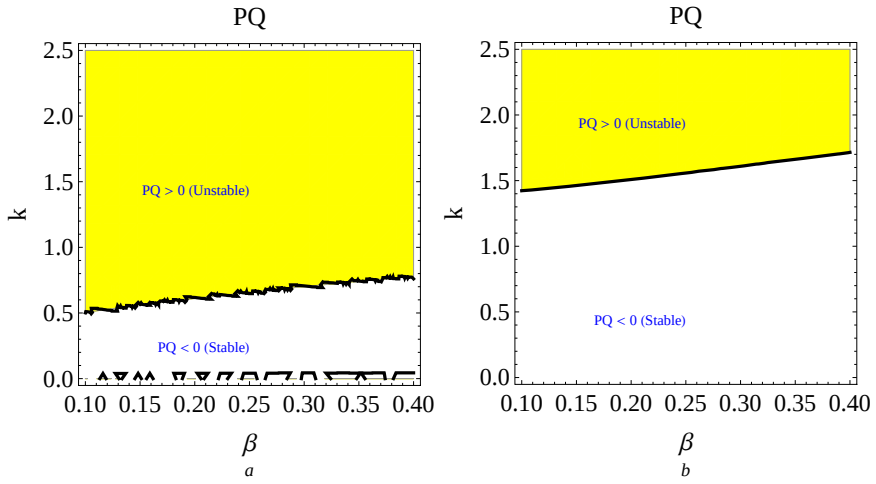

Fig. 5 – (color online) The regions of stable and unstable envelope wave packets according to the sign of the product PQ are depicted against the wave number k and the ratio of the effective temperature to ion temperature β for (a) the slow mode and (b) the fast mode. Here, $\mu = 0.6$, $\alpha = 0.5$, $\theta = 30^{\circ}$, and $\delta = 0.3$.

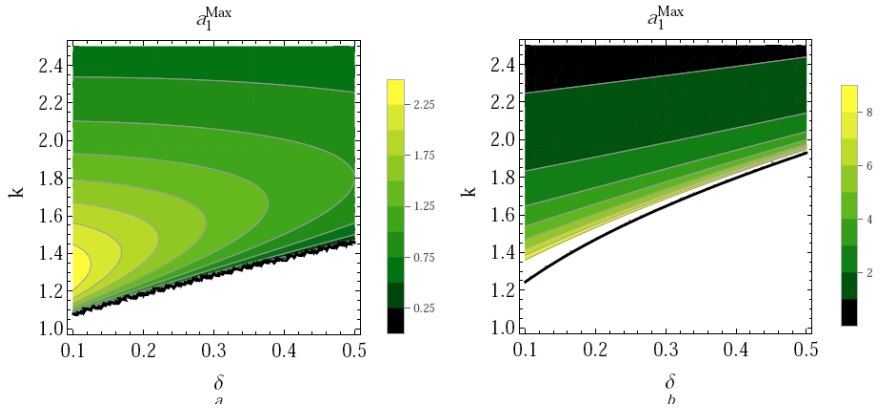

Fig. 6 – (color online) The contour of the maximum RW amplitude a_1 is depicted against the wave number k and the electron to dust density concentration δ for (a) the slow mode (dust-acoustic mode) and (b) the fast mode (dust-cyclotron mode). Here, $\alpha = 0.5$, $\beta = 0.3$, $\mu = 0.8$, and $\theta = 30^\circ$.

5. FREAK WAVE SOLUTION

It is known since long time that many nonlinear evolution equations such as the standard NLSE could describe a series of nonlinear wave phenomena [54–64]. This equation is ubiquitous describing propagation of the wave packet in nonlinear dispersive media. It has many nonlinear solutions and in our present study we focus our attention on a special unstable solution. Within the MI regions ($PQ > 0$), a random perturbation of the amplitude grows and thus may generate/create dust-acoustic and dust-ion cyclotron freak waves in the present plasma system. Many FWs experiments have suggested that the rational solutions of a NLSE indeed describe FW phenomena well. The experimental observation of fundamental (first-order) RWs in a multicomponent plasma with negative ions were reported. The measured amplitude of the first-order RWs is found to be more than twice the surrounding wave height. Moreover, the experimental observations agree with the theoretical results that obtained from the rational solution of the NLSE. After that and more recently, the second-order ion-acoustic RWs in multicomponent plasma with negative ions have been investigated experimentally. It was found that the wave focuses its energy into a small region, which makes the amplitude amplification up to 5 times of the background carrier wave. The experimental results are compared with second-order rogue wave (RW) solution of the NLSE. It was found that the theoretical results are in excellent agreement with the laboratory experiments.

The general rational solution of the NLSE (79) can be written in the following

form [65–67]

$$a_j(\eta,\bar{\tau}) \equiv a_j = \sqrt{\frac{P}{Q}}\left[(-1)^j + \frac{G_j(\eta,\bar{\tau}) + i\bar{\tau}H_j(\eta,\bar{\tau})}{F_j(\eta,\bar{\tau})}\right]\exp(i\bar{\tau}), \tag{83}$$

where j is the order of the freak wave solutions and $\bar{\tau} = P\tau$. Here $G_j(\eta,\bar{\tau})$, $H_j(\eta,\bar{\tau})$, and $F_j(\eta,\bar{\tau}) \neq 0$ are polynomials in the independent slow variables η and τ. Solution (83) represents the profile of the FWs in the unstable region ($PQ > 0$), which focuses a significant amount of energy into a small area in space, and therefore the FWs can be generated and propagated in the present plasma system in future experiments. Higher-order solutions of RWs (super RWs) are progressively more complicated. Therefore, we are dealing only with the first two orders $(j = 1 \text{ and } 2)$ because the higher orders have the same qualitative behavior.

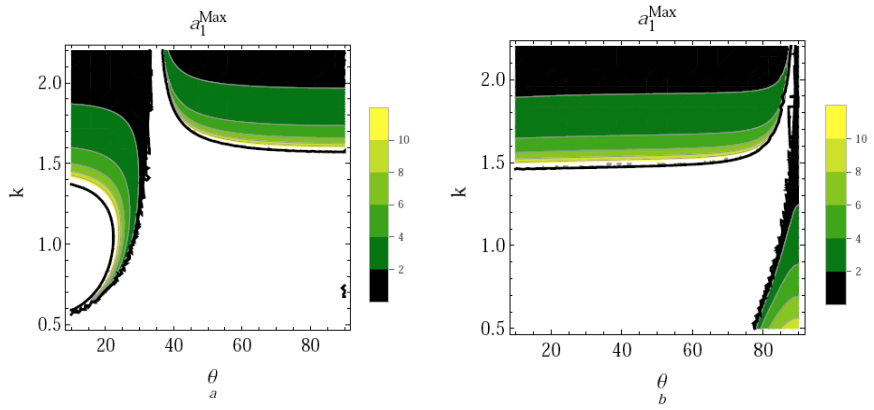

Fig. 7 – (color online) The contour of the maximum RW amplitude a_1 is depicted against the wave number k and the wave propagation angle θ for (a) the slow mode and (b) the fast mode. Here, $\alpha = 0.5$, $\beta = 0.3$, $\mu = 0.8$, and $\delta = 0.2$.

The polynomials for the first-order solution $(j = 1)$ have the following form [65, 66, 68]

$$H_1(\eta,\bar{\tau}) = 8,$$
$$G_1(\eta,\bar{\tau}) = 4,$$
$$F_1(\eta,\bar{\tau}) = 1 + 4\eta^2 + 4\bar{\tau}^2.$$

This solution refers to the fundamental RWs and sometimes is called the Peregrine soliton. The amplitude amplification of this solution equals three times the height of the carrier wave, *i.e.*, $a_1(0,0) \equiv a_1^{Max} = 3\sqrt{P/Q}$. The superposition of fundamental RWs a_1 provides the higher-order (super) solutions. Physically, the fundamental RWs sucked energy from the background waves and thus concentrate it into a rel-

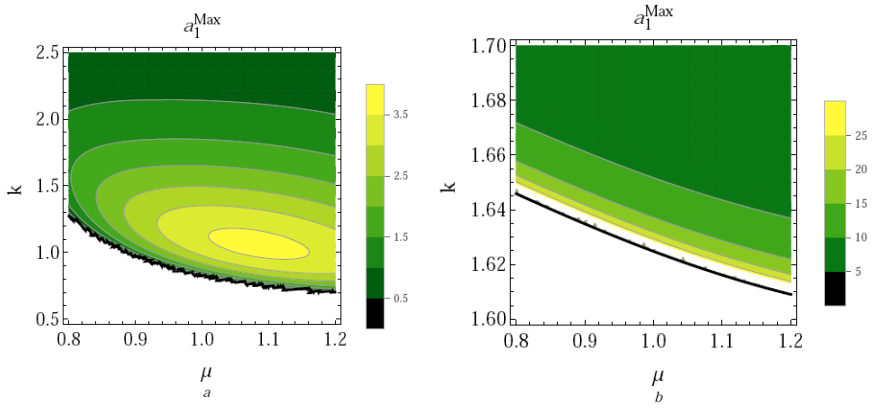

Fig. 8 – (color online) The contour of the maximum RW amplitude a_1 is depicted against the wave number k and the magnetic field intensity μ for (a) the slow mode and (b) the fast mode. Here, $\alpha = 0.5$, $\beta = 0.3$, $\theta = 30^{\circ}$, and $\delta = 0.3$.

atively small area, but super RW solutions sucked more energy from many places rather than a_1. So, it is expected that the super RW has a higher amplitude than the first-order solution.

The polynomials for the second-order/super RW solution $(j = 2)$ are given by [65–67]

$$G_2(\eta,\bar{\tau}) = \frac{3}{8} - 3\eta^2 - 2\eta^4 - 9\bar{\tau}^2 - 12\left(\eta\bar{\tau}\right)^2 - 10\bar{\tau}^4,$$
$$H_2(\eta,\bar{\tau}) = \frac{15}{4} + 6\eta^2 - 4\eta^4 - 2\bar{\tau}^2 - 8\left(\eta\bar{\tau}\right)^2 - 4\bar{\tau}^4,$$
$$F_2(\eta,\bar{\tau}) = \frac{1}{8}\left[\frac{3}{4} + 9\eta^2 + 4\eta^4 + \frac{16}{3}\eta^6 + 33\bar{\tau}^2 - 24\left(\eta\bar{\tau}\right)^2 + 16\left(\eta^2\bar{\tau}\right)^2 + 16\left(\eta\bar{\tau}^2\right)^2 + 36\bar{\tau}^4 + \frac{16}{3}\bar{\tau}^6\right].$$

The amplitude amplification of the second-order solution equals five times the height of the carrier wave, *i.e.*, $a_2(0,0) \equiv a_2^{Max} = 5\sqrt{P/Q}$.

To have a complete picture about the RW profile, the effects of electron to dust density concentration ratio δ, magnetic field intensity μ, temperature ratios of electrons and ions, respectively, α, β, and the carrier wave number k on the characteristics of the electrostatic RWs a_j in a magnetized dusty plasma are examined. Figures 6a and 6b show the effects of the electron concentration δ on the RW profile for slow and fast electrostatic modes in a magnetized dusty plasma, respectively. It is obvious that the RW amplitude decreases with the increase of δ for all values of permissible wave number and for slow mode (DAW), because the nonlinearity decreases

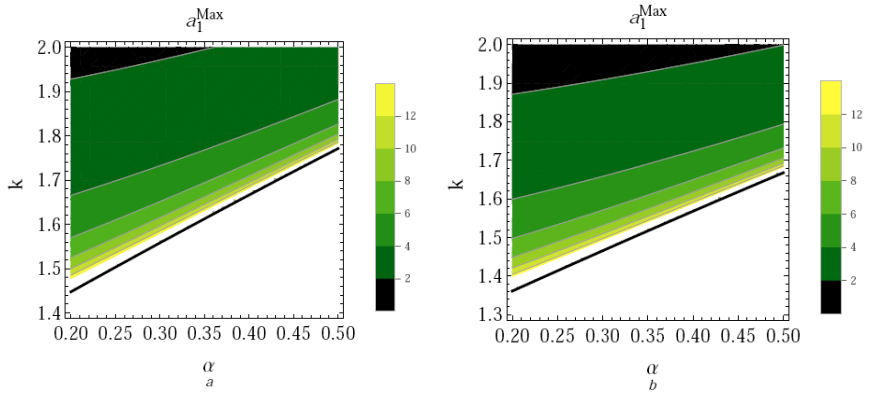

Fig. 9 – (color online) The contour of the maximum RW amplitude a_1 is depicted against the wave number k and the ratio of the effective temperature to electron temperature α for (a) the slow mode and (b) the fast mode. Here, $\mu = 0.6$, $\beta = 0.3$, $\theta = 30^{\circ}$, and $\delta = 0.3$.

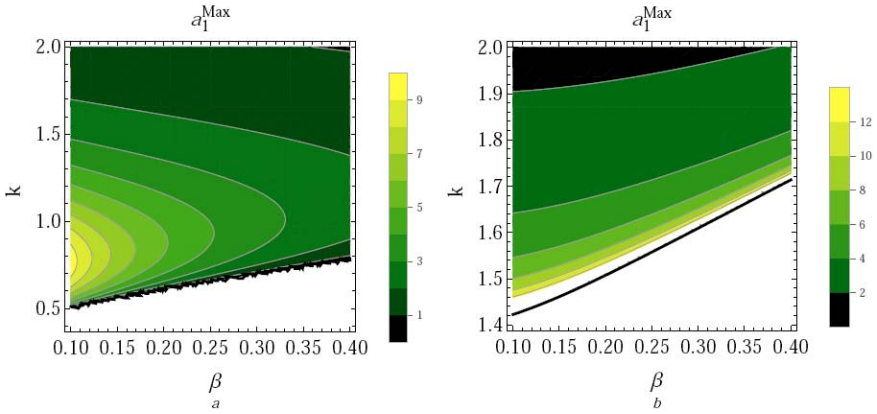

Fig. 10 – (color online) The contour of the maximum RW amplitude a_1 is depicted against the wave number k and the ratio of the effective temperature to ion temperature β for (a) the slow mode (DAW) and (b) the fast mode (DCW). Here, $\mu = 0.6$, $\alpha = 0.5$, $\theta = 30^{\circ}$, and $\delta = 0.3$.

due to the dissipation energy of the system. But for fast mode (DCW), it has opposite behavior. Furthermore, increasing the wave number k would increase the amplitude of the dust-acoustic RWs until it approaches a certain value; then a further increase in k decreases the RW amplitude, *i.e.*, for low values of k, increasing k enhances the nonlinearity and disperses and therefore increases the energy, which makes the pulses taller. However, for high values of k, the RW amplitude damps with the enhancement of k. On the other side for fast mode (DCW), increasing the wave number k would reduce the amplitude of the dust-cyclotron RW, *i.e.*, the system reduces its nonlinearity, which makes the pulses shorter. Moreover, for DCW, near the critical

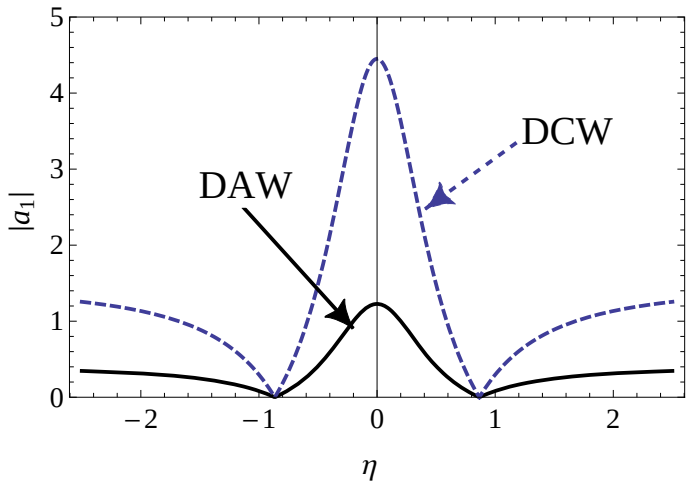

Fig. 11 – (color online) Comparison between the dust-acoustic RW and the dust-cyclotron RW. Here, $k = 1.4$, $\beta = 0.3$, $\mu = 0.8$, $\alpha = 0.5$, $\theta = 30^{\circ}$, and $\delta = 0.3$ at $\tau = 0$.

wave number K_c, the RW amplitude becomes taller because the instability pumps more energy into the system, which causes the enhancement of the nonlinearity and makes the pulses taller. Figure 7a depicts that for slow mode, the RW amplitude shrinks with the increase of θ and k. On the contrary, for the fast mode, the RW amplitude grows with the increase of θ but decreases with the increase of k as shown in Fig. 7b. The variation of magnetic field intensity μ on RW properties is depicted in Fig. 8. For the slow mode (DAW), it is seen from Fig. 8a that the increase of μ would increase the nonlinearity and then concentrates a significant amount of energy into a small area, which leads to an increase of the pulses amplitude for small wave number. However, for large wave number, increasing μ leads to a reduction of the nonlinearity and then dissipates the system energy, which leads to a shrinkage the pulses amplitude. For the fast mode (DCW), one can see that the pulses amplitude always decreases with the increase of μ as elucidated in Fig. 8b. It is interesting to examine the behavior of the RW amplitude near the critical wave number. First, for DAW, it is obvious from Fig. 8a that the RW amplitude decreases, but for DCW, near to the critical wave number, the wave amplitude increases because the wave concentrates a significant amount of energy from the surrounding waves that makes the pulses taller; however, as we are far away from the critical wave number the system loses its energy, which reduces the nonlinearity and the pulses become shorter. The dependence of the RW amplitude on the electrons temperature ratio α is depicted in Figs. 9a and 9b for DAW and DCW, respectively. It is observed that the RW amplitude always increases (decreases) for both modes with the enhancement of α (k). Figures 10a and 10b depict the variation of the RW amplitude with the ions temper-

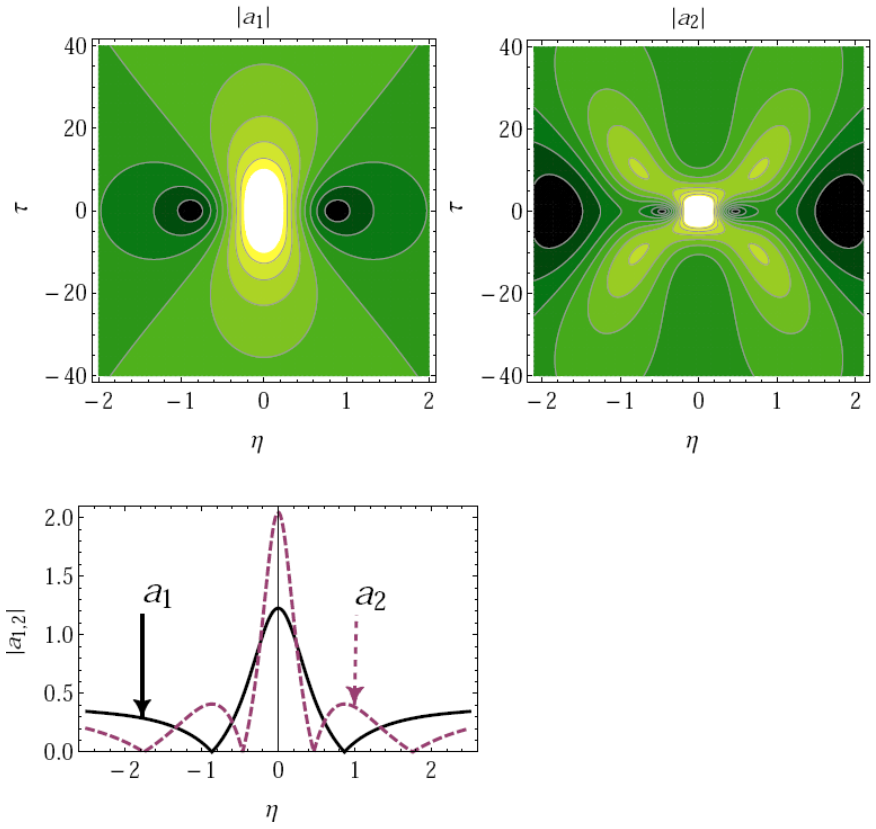

Fig. 12 – (color online) Comparison between the fundamental (first-order) RW and the super (second-order) RW. Here, $k = 1.5$, $\beta = 0.2$, $\mu = 1.2$, $\alpha = 0.5$, $\theta = 30^{\circ}$, and $\delta = 0.3$ at $\tau = 0$.

ature ratio β for slow and fast mode, respectively. It is seen that the amplitude of the two modes has similar behavior as in Fig. 6. It is noted from the above figures that the RW amplitude and width of DCW are larger than DAW as depicted in Fig. 11. In general, when the nonlinearity of the system decreases, the system dissipates its energy and the wave amplitude damps. On the contrary, increasing the nonlinearity of the system would enhance the energy and concentrate it into a small area, which makes the pulses taller.

Figure 12 illustrates a comparison between the first- and second-order RW solution of the NLSE (79). Note that the second-order solution a_2 has double structures compared with the first-order solution a_1. Further, one notices that for the same physical parameters, the second-order solution a_2 is much spiky (taller amplitude and narrower width) than the first-order solution a_1, which indicates that a_2 sucks more energy from the surrounding waves.

6. CONCLUSION

We have investigated the modulational instability and the electrostatic structures (*i.e.*, freak waves) in a three-component magnetized dusty plasma composed of negatively charged dust grains and Maxwellian distributed electrons and ions. The Krylov-Bogoliubov-Mitropolsky method is used to derive the nonlinear Schrödinger equation that governs the dynamics of modulated wave packets and envelope structures. The modulationally stable (white regions) and unstable (shaded regions) for dust-acoustic wave (DAW) and dust-cyclotron waves (DCW) are examined numerically. The dependence of modulated unstable regions of DAW and DCW on various plasma parameters such as wave propagation angle θ, ratio of electron to dust density concentration δ, ratio of effective temperature to electron temperature α, ratio of effective temperature to ion temperature β, the magnetic field intensity μ, and the carrier wave number k is investigated. It is found that for low values of wave number, the nonlinear dust-acoustic and dust-cyclotron wave packets are structurally stable. However, for large wave numbers the situation is opposite. This study shows that the present plasma system would introduce unique features for the nonlinear modulated wave packets, which do not exist in an unmagnetized dusty plasma. It is noticed that a small instability region for the fast mode is formed as compared to the slow one case. Within the modulational unstable regions, a random perturbation of the amplitude grows and thus leads to the creation of the dust-acoustic and dust-cyclotron freak waves. The dependence of the freak waves for the slow and fast modes on the relevant physical parameters is numerically examined. Our present investigation is applicable to magnetized space plasmas and in laboratory experiments where negatively charged dust particles can exist [15].

APPENDIX

A): Derivation of the solution of Φ_2

Derivation of the second order solution for Φ_2 of Eq. (53), which is a nonhomogeneous differential equation, has two solutions: (i) characteristic Φ_{2c} and (ii) particular Φ_{2p} *i.e.*,

$$\Phi_2 = \Phi_{2c} + \Phi_{2p}. \tag{a-1}$$

For Φ_{2c} the equation can be written as

$$\left(y_1 D^2 - y_2\right)\left(D^2 + 1\right) = 0, \tag{a-2}$$

where y_1, y_2, and operator D are defined after Eqs. (41) and (44). The roots of the homogenous part of the differential equation (53) are obtained as

$$\left(y_1 m^2 - y_2\right)\left(m^2 + 1\right) = 0. \tag{a-3}$$

$$m = \pm i,\ \pm\sqrt{y_2/y_1}. \tag{a-4}$$

So we have the characteristic solution in the form

$$\Phi_{2c} = C_1 e^{i\psi} + C_1^{'} e^{-i\psi} + C_2 e^{\sqrt{y_2/y_1}\psi} + C_3 e^{-\sqrt{y_2/y_1}\psi}. \tag{a-5}$$

Here C_1 is constant and $C_1^{'}$ is complex conjugate of C_1, while C_2 and C_3 are constants. For different ranges of parameters, y_2/y_1 can have both positive as well as negative values. If y_2/y_1 is positive, for long time *i.e.*, $\psi = kx - \omega t$, then $e^{-\sqrt{y_2/y_1}\psi}$ becomes secular while $e^{\sqrt{y_2/y_1}\psi}$ becomes small and get damped. However, if y_2/y_1 is negative, then these terms have to be dropped out at $O\left(\epsilon^3\right)$ in order to have a secularity free solution of Φ_2. Therefore, we have

$$\Phi_{2c} = b\left(a, \bar{a}\right) e^{i\psi} + c.c, \tag{a-6}$$

where the constant $C_1 = b(a, \bar{a})$ is defined as an arbitrary function that appears in solution of Φ_2 given in Eq. (55).

For particular solution, we have to separate Eq. (53) into three parts as follows

$$\left(y_1 D^2 - y_2\right)\left(D^2 + 1\right)\Phi_{2p1} = Z_1 a^2 e^{2i\psi}, \tag{a-7}$$

$$\left(y_1 D^2 - y_2\right)\left(D^2 + 1\right)\Phi_{2p2} = Z_1 \bar{a}^2 e^{-2i\psi}, \tag{a-8}$$

$$\left(y_1 D^2 - y_2\right)\left(D^2 + 1\right)\Phi_{2p3} = c_1^{''}, \tag{a-9}$$

where

$$Z_1 = \left(1 - 4\omega^2\mu^2\right)\left[\omega^2\Gamma^2 + \frac{k^2\cos^2\theta}{2}\Gamma - \frac{\omega^2\left\{\left(1+\delta\right)\beta^2 - \delta\alpha^2\right\}}{2}\right]$$
$$- \Gamma\left(1 + 2\omega^2\mu^2\right)\left(\omega^2\Gamma - k^2\cos^2\theta\right).$$

Now solution of Φ_{2p1} and Φ_{2p2} described in Eqs. (a-7) and (a-8) are complex conjugate of each other *i.e.*, $\Phi_{2p2} = \bar{\Phi}_{2p1}$. Let

$$\Phi_{2p1} = \rho_1 e^{2i\psi} \tag{a-10}$$

be the solution of Eq. (a-7), where ρ_1 is a constant and has to be found out. Putting (a-10) in Eq. (a-7), then we have

$$\left[y_1\left(2i\right)^2 - y_2\right]\left[\left(2i\right)^2 + 1\right]\rho_1 e^{2i\psi} = Z_1 a^2 e^{2i\psi}, \tag{a-11}$$

$$\left(-4y_1 - y_2\right)\left(-4 + 1\right)\rho_1 e^{2i\psi} = Z_1 a^2 e^{2i\psi}, \tag{a-12}$$

$$\rho_1 = \frac{Z_1 a^2}{3\left(4y_1 + y_2\right)}. \tag{a-13}$$

Therefore,

$$\Phi_{2p1} = \frac{Z_1 a^2}{3\left(4y_1 + y_2\right)} e^{2i\psi} = G a^2 e^{2i\psi}, \tag{a-14}$$

similarly following the same procedure, the solution of Φ_{2p2} is given by

$$\Phi_{2p2} = \bar{\Phi}_{2p1} = \frac{Z_1 \bar{a}^2}{3(4y_1 + y_2)} e^{-2i\psi} = G\bar{a}^2 e^{-2i\psi}, \tag{a-15}$$

where $G = \frac{Z_1}{3(4y_1+y_2)}$, which is the same as defined in Eq. (56).

The solution of (a-8) is

$$\Phi_{2p3} = \rho_2. \tag{a-16}$$

Now using the above solution in (a-9), we have

$$(0 - y_2)(0+1)\rho_2 = c_1^{''}, \tag{a-17}$$

$$\rho_2 = -\frac{c_1^{''}}{y_2} = c_1. \tag{a-18}$$

Therefore, the solution of the nonhomogeneous part of the differential Eq. (53) is given by

$$\Phi_{2p} = \Phi_{2p1} + \Phi_{2p2} + \Phi_{2p3}, \tag{a-19}$$

$$\Phi_{2p} = Ga^2 e^{2i\psi} + c.c + c_1. \tag{a-20}$$

The complete solution of Φ_2 is

$$\Phi_2 = \Phi_{2c} + \Phi_{2p}, \tag{a-21}$$

$$\Phi_2 = Ga^2 e^{2i\psi} + b(a,\bar{a}) e^{i\psi} + c.c + c_1(a,\bar{a}). \tag{a-22}$$

We will see further that collecting secular terms at higher order *i.e.*, $O\left(\epsilon^3\right)$ to find NLSE in which coefficients with terms $e^{\pm i\psi}$ are collected, the terms containing $b(a,\bar{a})$ get cancelled out while other terms gives NLSE.

B): The expressions of parameters defined in Eq. (57)

The parameters defined in Eq. (57) are described as follows

$$G_1 = \left[\frac{(1+\delta)\beta^2 - \delta\alpha^2}{2}\right] - \left(\Gamma + 3k^2\right) G, \tag{b-1}$$

$$G_2 = \frac{1}{\sin\theta}\left\{\frac{\omega}{k}G_1 - \frac{\omega}{k}\Gamma^2 - \frac{k\cos^2\theta}{2\omega}(\Gamma - 2G)\right\}, \tag{b-2}$$

$$G_3 = \frac{-i}{2\mu\omega}\left[\Gamma N_2 - \frac{1}{\sin\theta}\left\{\frac{\omega}{k}G_1 - \frac{\omega}{k}\Gamma^2 - \frac{k\cos^2\theta}{2\omega}(\Gamma - 2G)\right\}\right], \tag{b-3}$$

$$G_4 = \frac{k\cos\theta}{2\omega}(\Gamma - 2G), \tag{b-4}$$

$$G_5 = \left(\frac{\omega}{k}G_1 - \frac{\omega}{k}\Gamma^2\right), \tag{b-5}$$

$$\Xi_1 = 2ikB_1, \tag{b-6}$$

$$\Xi_2 = \frac{1}{\sin\theta}\left[\frac{\omega}{k}\Sigma_1 - i\left(A_1 + \frac{\omega}{k}B_1\right)\frac{\Gamma}{k} - \frac{i}{\omega}\left(\frac{k}{\omega}A_1 + B_1\right)\cos^2\theta\right], \tag{b-7}$$

$$\Xi_3 = \frac{-i}{\mu\omega}\left[\frac{iN_2}{\omega}A_1 - \frac{1}{\sin\theta}\left\{\frac{\omega}{k}\Sigma_1 - i\left(A_1 + \frac{\omega}{k}B_1\right)\frac{\Gamma}{k} - \frac{i}{\omega}\left(\frac{k}{\omega}A_1 + B_1\right)\cos^2\theta\right\}\right], \tag{b-8}$$

$$\Xi_4 = \frac{i}{\omega}\left(\frac{k}{\omega}A_1 + B_1\right)\cos\theta, \tag{b-9}$$

$$\Xi_5 = \frac{\omega}{k}\Sigma_1 - i\left(A_1 + \frac{\omega}{k}B_1\right)\frac{\Gamma}{k}. \tag{b-10}$$

REFERENCES

1. E. C. Whipple, T. G. Northrop, and D. A. Mendis, J. Geophys. Res. **90**, 7405–7413 (1985).
2. C. K. Goertz, Rev. Geophys. **27**, 271–292 (1989).
3. A. Barkan, R. L. Merlino, and N. D' Angelo, Phys. Plasmas **2**, 3563–3565 (1995).
4. F. Verheest, Space Sci. Rev. **77**, 267–302 (1996).
5. M. Horányi, G. Morfill, and E. Grün, Nature (London) **363**, 144 (1993).
6. P. K. Shukla and A. A. Mamun *Introduction to Dusty Plasma Physics*, Bristol IOP, 2002, p. 93.
7. S. Benkadda, V. N. Tsytovich, and A. Verga, Comments on Plasma Phys. Controlled Fusion **16**, 321–333 (1995).
8. N. D' Angelo, Planet. Space Sci. **50**, 375–378 (2002).
9. P. K. Shukla and M. Rosenberg, Phys. Scr. **73**, 196 (2006).
10. A. A. Mamun and P. K. Shukla, Geophys. Res. Lett. **29**, 17 (2002).
11. F. Sayed and A. A. Mamun, Phys. Plasmas **14**, 014501 (2007).
12. R. Bingham, U. de Angelies, V. N. Tsytovich, and O. Havnes, Physics of Fluids B: Plasma Physics, **3**, 811–817 (1991).
13. Y. N. Nejob, Phys. Plasmas **4**, 2813 (1997).
14. B. S. Xie, K. F. He, and Z. Huang, Chin. Phys. Lett. **17**, 815 (2000).
15. N. N. Rao, P. K. Shukla, and M. Y. Yu, Planet Space Sci. **38**, 691 (1990).
16. P. K. Shukla and V. P. Silin, Phys. Scr. **45**, 508 (1992).
17. G. E. Morfill and H. Thomas, J. Vac. Sci. Technol. **A14**, 490-495 (1996).
18. R. L. Merlino, A. Barkan, C. Thompson, and N. D' Angelo, Planet. Space Sci. **38**, 1143–1146 (1990).
19. N. Akhtar, S. Mahmood, and H. Saleem, Phys. Lett. A **361**, 126–132 (2007).
20. H. Zhang, Y. Yang, X.-R. Hong, X. Qi, W.-S. Duan, and L. Yang, Phys. Rev. E **95**, 053207 (2017).
21. W. S. Duan, J. Parkes, and L. Zhang, Phys. Plasmas **11**, 3761 (2004).
22. M. R. Amin, G. E. Morfill, and P. K. Shukla, Phys. Rev. E **58,** 6517 (1998).
23. J. Xue and L. He, Phys. Plasmas **10**, 339–342 (2003).
24. I. Kourakis and P. K. Shukla, Phys. Plasmas **10**, 3459 (2003).
25. H. R. Pakzad, K. Javidan, and A. Rafiei, Astrophys. Space Sci. **353**, 543–550 (2014).
26. T. S. Gill, A. S. Bains, and C. Bedi, Phys. Plasmas **17**, 013701 (2010).
27. N. Akhtar, and S. Mahmood, IEEE Transactions on Plasma Sci. **44**, 2907–2914 (2016).
28. T. Kakutani and N. Sugimoto, Phys. Fluids **17**, 1617–1625 (1974).
29. M. Salahuddin, H. Saleem, and M. Sadiq, Phys. Rev. E **66**, 36407 (2002).
30. N. Jehan, M. Salahuddin, H. Saleem, and A. M. Mirza, Phys. Plasmas **15**, 092301 (2008).
31. S. Mahmood, S. Siddiqui, and N. Jehan, Phys. Plasmas **18**, 052309 (2011).

32. S. A. El-Tantawy and Tarek Aboelenen, Phys. Plasmas **24**, 052118 (2017).
33. X. Lü, W. X. Ma, J. Yu, F. Lin, and C. M. Khalique, Nonlinear Dyn. **82**, 1211-1220 (2015).
34. B. Sun and A. M. Wazwaz, Commun. Nonlinear Sci. Numer. Simul. **64**, 1–13 (2018).
35. M. Bertola, G. A. El, and A. Tovbis, Proc. R. Soc. A **472**, 20160340 (2016).
36. M. S. Ruderman, T. Talipova, and E. Pelinovsky, J. Plasma Phys. **74**, 639–656 (2008).
37. M. S. Ruderman, Eur. Phys. J. Spec. Top. **185**, 57-66 (2010).
38. M. Onorato, S. Residori, U. Bortolozzo, A. Montina, and F. T. Arecchi, Phys. Rep. **528**, 47–89 (2013).
39. M. Onorato, D. Proment, G. Clauss, and M. Klein, PLoS ONE **8**, e54629 (2013).
40. S. Chen, F. Baronio, J. M. Soto-Crespo, P. Grelu, and D. Mihalache, J. Phys. A: Math. Theor. **50**, 463001 (2017).
41. D. Mihalache, Rom. Rep. Phys. **69**, 403 (2017).
42. J. S. He, S. W. Xu, K. Porsezian, P. T. Dinda, D. Mihalache, B. A. Malomed, and E. Ding, Rom. J. Phys. **62**, 203 (2017).
43. W. Liu, Rom. J. Phys. **62**, 118 (2017).
44. Yongshuai Zhang, Lijuan Guo, Amin Chabchoub, and Jingsong He, Rom. J. Phys. **62**, 102 (2017).
45. S. Chen, Y. Zhou, F. Baronio, and D. Mihalache, Rom. Rep. Phys. **70**, 102 (2018).
46. W. Liu, Y. Zhang, and J. He, Rom. Rep. Phys. **70**, 106 (2018).
47. Shalini, A. P. Misra, and N. S. Saini, J. Theor. Appl. Phys. **11**, 217–224 (2017).
48. S. Guo and L. Mei, Phys. Plasmas **21**, 82303 (2014).
49. N. Akhtar, S. Mahmood, N. Jehan, and A. M. Mirza, Phys. Plasmas **24**, 113707 (2017).
50. G. Tagare, and A. S. Sharma, Phys. Fluids **19**, 762–763 (1976).
51. T. Kakutani and N. Sugimoto, Phys. Fluids **17**, 1617–1625 (1974).
52. K. Nishikawa and C. S. Liu, Advances in Plasma Physics **6**, Wiley, New York, 1976, p. 59.
53. J. K. Chawla, M. K. Mishra, and R. S. Tiwari, Astrophys. Space Sci. **347**, 283–292 (2013).
54. A. M. Wazwaz, *Partial Differential Equations: Methods and Applications*, Balkema Publishers, The Netherlands, 2002.
55. H. Triki and A. M. Wazwaz, Rom. J. Phys. **61**, 360–366 (2016).
56. A. M. Wazwaz, Math. Comput. Modelling **43**, 178–184 (2006).
57. A. M. Wazwaz, Math. Comput. Modelling **43**, 802–808 (2006).
58. A. M. Wazwaz, Chaos, Solitons and Fractals **37**, 1136–1142 (2008).
59. Q. Zhou, Proc. Romanian Acad. A **18**, 223–230 (2017).
60. Yongshuai Zhang, Deqin Qiu, Yi Cheng, and Jingsong He, Rom. J. Phys. **62**, 108 (2017).
61. P. F. Li and D. Mihalache, Proc. Romanian Acad. A **19**, 61–68 (2018).
62. A. M. Wazwaz, Rom. Rep. Phys.**69**, 108 (2017).
63. R. Constantinescu, Rom. Rep. Phys. **69**, 112 (2017).
64. M. T. Darvishi, M. Najafi, and A. M. Wazwaz, Rom. Rep. Phys. **70**, 108 (2018).
65. S. A. El-Tantawy, N. A. El-Bedwehy, and S. K. El-Labany, Phys. Plasmas **20**, 072102 (2013).
66. S. A. El-Tantawy, N. A. El-Bedwehy, and W. M. Moslem, J. Plasma Physics **79**, 1049-1056 (2013).
67. N. Akhmediev, A. Ankiewicz, and J. M. Soto-Crespo, Phys. Rev. E **80**, 026601 (2009).
68. S. A. El-Tantawy and W. M. Moslem, Phys. Plasmas **21**, 052112 (2014).